

# Geophysical Research Letters<sup>®</sup>



## RESEARCH LETTER

10.1029/2023GL103381

## Overturning Pathways Control AMOC Weakening in CMIP6 Models

### Key Points:

- The magnitude of 21st century Atlantic Meridional Overturning Circulation (AMOC) weakening in CMIP6 models is highly correlated with an AMOC pathway into the Indo-Pacific Ocean
- The real-world “Indo-Pacific diffusive” AMOC pathway inferred from observation-based estimates is used to constrain future AMOC weakening
- Under high-end greenhouse gas forcing, AMOC weakening based on this emergent constraint relationship ranges from 29% to 61% by 2100

### Supporting Information:

Supporting Information may be found in the online version of this article.

### Correspondence to:








J. A. Baker,  
[jonathan.baker@metoffice.gov.uk](mailto:jonathan.baker@metoffice.gov.uk)

### Citation:

Baker, J. A., Bell, M. J., Jackson, L. C., Renshaw, R., Vallis, G. K., Watson, A. J., & Wood, R. A. (2023). Overturning pathways control AMOC weakening in CMIP6 models. *Geophysical Research Letters*, 50, e2023GL103381. <https://doi.org/10.1029/2023GL103381>

Received 21 FEB 2023

Accepted 30 JUN 2023

Jonathan A. Baker<sup>1</sup> , Michael J. Bell<sup>1</sup> , Laura C. Jackson<sup>1</sup> , Richard Renshaw<sup>1</sup> ,  
Geoffrey K. Vallis<sup>2</sup> , Andrew J. Watson<sup>2</sup> , and Richard A. Wood<sup>1</sup> 

<sup>1</sup>Met Office, Exeter, UK, <sup>2</sup>University of Exeter, Exeter, UK

**Abstract** Future projections indicate the Atlantic Meridional Overturning Circulation (AMOC) will weaken and shoal in response to global warming, but models disagree widely over the amount of weakening. We analyze projected AMOC weakening in 27 CMIP6 climate models, in terms of changes in three return pathways of the AMOC. The branch of the AMOC that returns through diffusive upwelling in the Indo-Pacific, but does not later upwell in the Southern Ocean (SO), is particularly sensitive to warming, in part, because shallowing of the deep flow prevents it from entering the Indo-Pacific via the SO. The present-day strength of this Indo-Pacific pathway provides a strong constraint on the projected AMOC weakening. However, estimates of this pathway using four observationally based methods imply a wide range of AMOC weakening under the SSP5-8.5 scenario of 29%–61% by 2100. Our results suggest that improved observational constraints on this pathway would substantially reduce uncertainty in 21st century AMOC decline.

**Plain Language Summary** The Atlantic Meridional Overturning Circulation (AMOC) is a system of ocean currents that move warm surface waters from the south to the north of the Atlantic Ocean where they cool, sink, and return southward at depth. Changes in the AMOC would have wide-ranging impacts on our climate. It is predicted to weaken as the climate warms during the 21st century, but the extent of weakening varies among different climate models. We show that AMOC weakening is greatest in models that have a large exchange of water between the AMOC and the Indo-Pacific Ocean along a specific pathway. The magnitude of this ocean pathway, inferred from four observation-based estimates of the global overturning circulation, is uncertain. By using these estimates and analyzing the relationship between the aforementioned ocean pathway and AMOC weakening across many climate models, we can predict how the real-world AMOC will change. Our findings indicate that by 2100, under a high greenhouse gas emission scenario, the AMOC will weaken by 29%–61%. This highlights the importance of reducing differences between observational estimates of the ocean's overturning pathways to reduce uncertainty in future AMOC weakening and to improve the representation of these pathways in climate models.

## 1. Introduction

The Atlantic Meridional Overturning Circulation (AMOC) is widely predicted to weaken over the 21st century (e.g., Cheng et al., 2013; Weijer et al., 2020), but the magnitude of this change is uncertain in the Coupled Model Intercomparison Project Phase 6 (CMIP6). Understanding the mechanisms responsible for the large inter-model spread is crucial to predict the transient response of the AMOC to increased greenhouse gas (GHG) concentrations. The ocean's overturning pathways are an important determinant of the equilibrium response of the AMOC to climate forcing (Baker et al., 2020, 2021; Nadeau & Jansen, 2020) and they may therefore also play a role in determining its transient response. We hypothesize that the wide range in the AMOC's transient response to climate forcing among CMIP6 models is due to differences in the historical magnitude of their overturning pathways.

Changes in the Meridional Overturning Circulation (MOC) influence global and regional climate change on seasonal to millennial timescales by changing the ocean's transport of heat, freshwater, and carbon (Buckley & Marshall, 2016; Rahmstorf, 2015; Weijer et al., 2019). How the AMOC changes over the 21st century will impact many aspects of the climate (Bellomo et al., 2021; Hu et al., 2020; Liu et al., 2020), so constraining its future response to warming is vital.

The most comprehensive predictions of future changes in climate are provided by CMIP6, a multi-model ensemble of climate simulations (Eyring et al., 2016; O'Neill et al., 2016). In model intercomparison projects, the

© 2023 Crown copyright and The Authors. This article is published with the permission of the Controller of HMSO and the King's Printer for Scotland. This is an open access article under the terms of the [Creative Commons Attribution-NonCommercial License](https://creativecommons.org/licenses/by-nc/4.0/), which permits use, distribution and reproduction in any medium, provided the original work is properly cited and is not used for commercial purposes.

weakening of the AMOC induced by increasing GHG forcing tends to be greater in models with a stronger control AMOC, so its present-day strength can be used to constrain future weakening (e.g., Cheng et al., 2013; Gregory et al., 2005; Weaver et al., 2012; Weijer et al., 2020; Winton et al., 2014). Several mechanisms have been proposed to explain this dependence. These include the impact of northern sea-ice extent and its subsequent retreat on North Atlantic Ocean heat loss (Levermann et al., 2007), changes in the kinetic energy of the North Atlantic (Gregory & Tailleux, 2011), changes in Labrador Sea convection (Rugenstein et al., 2013), and North Atlantic salinity differences (Jackson et al., 2020). These arguments are based on differences in the mean state and response of the North Atlantic that ultimately affect North Atlantic convection. In contrast, we use the CMIP6 ensemble to investigate the cause of the inter-model spread in AMOC weakening and its dependence on the historical AMOC strength by analyzing the model overturning pathways (e.g., Lumpkin & Speer, 2007; Talley, 2013) that return deep waters formed in the North Atlantic to the surface.

The pathways that return North Atlantic Deep Water (NADW) to the surface in the present-day ocean either upwell in the Southern Ocean (SO) driven by the SO westerly winds (e.g., Toggweiler & Samuels, 1998) or in the Atlantic and Indo-Pacific Oceans driven by diffusion (e.g., Munk & Wunsch, 1998). Diffusive upwelling in the Indo-Pacific Ocean may significantly impact the equilibrium state of the global overturning circulation, including the AMOC (Ferrari et al., 2017; Jones & Cessi, 2016; Newsom & Thompson, 2018; Thompson et al., 2016); however, its impact on the AMOC on shorter, transient timescales is unclear. Transient changes in the AMOC due to GHG forcing are believed to be instigated by changes in North Atlantic buoyancy forcing (Dixon et al., 1999; Stouffer et al., 2006), although the strengthening and poleward shift of the SO westerly winds found under high-end warming scenarios in CMIP6 models (Deng et al., 2022) may also impact the AMOC. In cooler, glacial climates, the equilibrium AMOC probably shoaled, decoupling the upper and lower cells of the MOC and thus isolating the AMOC from the Indo-Pacific Ocean (Baker et al., 2020, 2021; Ferrari et al., 2014; Nadeau & Jansen, 2020). The AMOC may also shoal in response to GHG forcing with its transient response investigated in idealized models (e.g., Bonan et al., 2022; Chang & Jansen, 2022; Sun et al., 2020). The Indo-Pacific overturning circulation responds rapidly to GHG forcing, weakening to compensate changes in the AMOC through communication between the North Atlantic and Indo-Pacific Oceans via wave processes (Sun et al., 2020).

By analyzing the historical overturning pathways and their response to varying GHG forcing, we can assess their impact, if any, on the transient response of the AMOC, and thus potentially constrain future changes in the real-world AMOC. These pathways correspond to the mechanisms responsible for the upwelling of deep waters formed in the North Atlantic (i.e., diffusive or wind-driven upwelling) and the regions where this upwelling occurs. We can therefore identify the processes that affect the transient weakening of the AMOC, such as changes in the SO westerly winds.

The main questions we seek to answer are:

- What are the historical overturning pathways in CMIP6 models and how do they change in a warmer climate?
- How do the historical overturning pathways affect the transient weakening of the AMOC, and what mechanisms are responsible for these dependencies?
- Can we use estimates of the real-world overturning pathways to constrain future AMOC weakening?

## 2. Data and Methods

### 2.1. CMIP6 Models and Observation-Based Data

We analyze the overturning pathways in the CMIP6 historical (1850–2014) simulation (Eyring et al., 2016) and in the Scenario Model Intercomparison Project (ScenarioMIP; O’Neill et al., 2016) experiments (2015–2100). The ScenarioMIP experiments represent different Shared Socioeconomic Pathways (SSPs; Riahi et al., 2017) that result in varying radiative forcing and thus warming by 2100. These range from low-end (SSP1-2.6 (“ssp126”)) to high-end (SSP5-8.5 (“ssp585”)) forcing scenarios. We focus on ssp585 since it has the largest AMOC response. The monthly mean overturning mass streamfunction that includes the Eulerian-mean and parameterized eddy components (Griffies et al., 2016) is produced by 49 models for the historical simulation, 26 models for ssp126 and 27 models for ssp585 (Table S1 in Supporting Information S1). We analyze the overturning streamfunction in depth space (variables, “msftmz” or “msftyz”), and in density space (variables, “msftmrho” or “msftyrho”) when it is available, using a single ensemble member from each model (Table S1 in Supporting Information S1). The overturning streamfunction represents the zonally integrated volume transport in latitude-depth space (Figures 1a

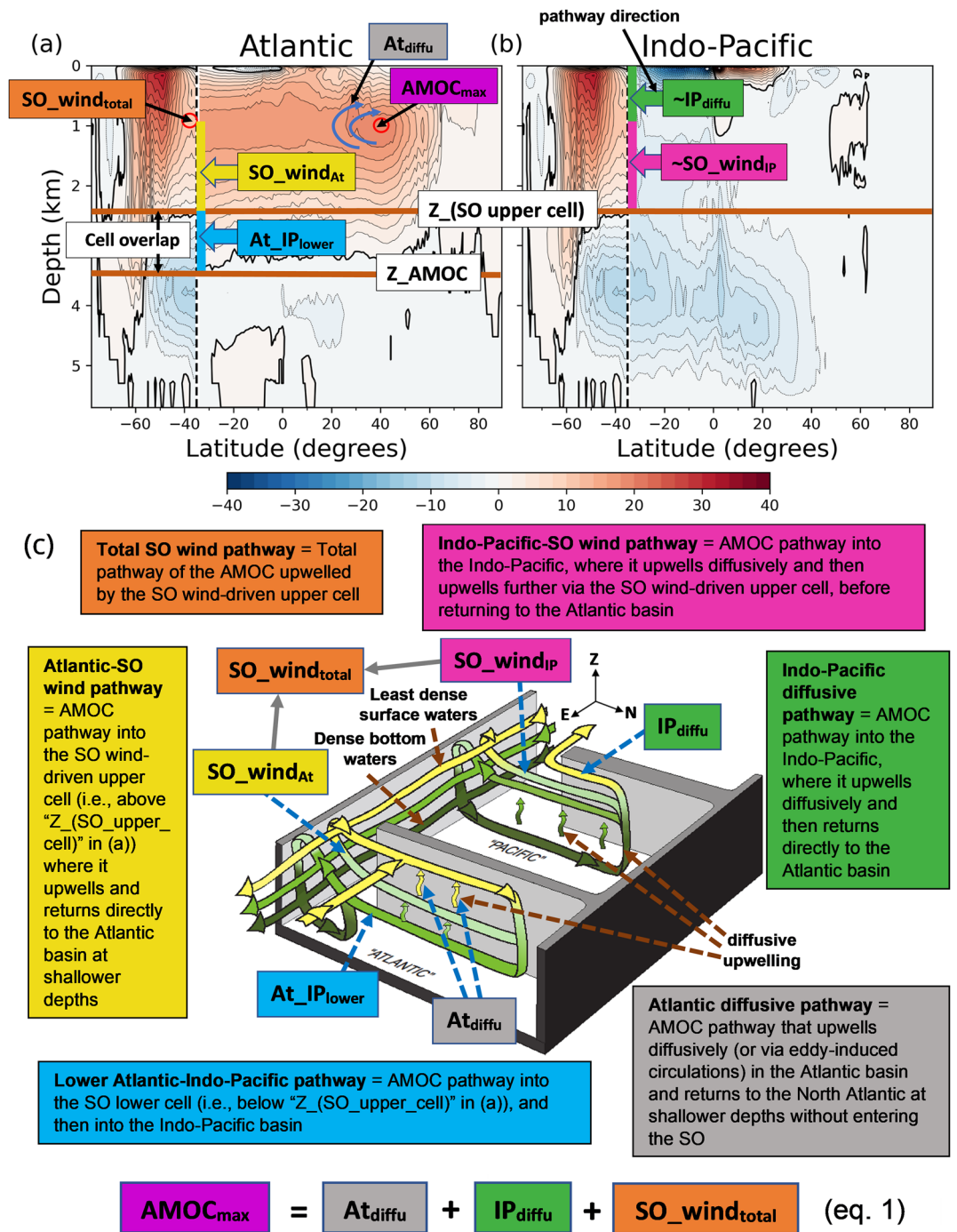


**Figure 1.** (a and b) Meridional overturning streamfunction (Sverdrups (Sv); 2 Sv contours) in the CMCC-ESM2 historical (1850–2014) simulation, illustrating the method used to separate the overturning pathways. North of 34.5°S (right-hand vertical dashed lines), the streamfunction is plotted for the model Atlantic (a) and Indo-Pacific (b). The globally integrated streamfunction is plotted in the Southern Ocean (SO). The solid black contour is the 0-Sv streamline. Each pathway, except “ $SO\_wind_{total}$ ” and “ $At_{diffu}$ ,” is the net volume of water flowing from the northern basin into the SO over the depth of the associated colored vertical line at 34.5°S. Red circles represent the Meridional Overturning Circulation strength at the highlighted location. Terms in white boxes are defined in Supporting Information S1 (Table S4). Note that we calculate the pathways shown in (b) as residuals using Equation 1 and Equation S5 in Supporting Information S1. (c) Illustration of the present-day overturning pathways. Each pathway is assigned a color and defined. The solid, gray arrows pointing to “ $SO\_wind_{total}$ ” show that this pathway is equal to the sum of “ $SO\_wind_{At}$ ” and “ $SO\_wind_{IP}$ .”

and 1b) and is calculated by integrating the meridional velocity zonally and vertically. We average the monthly mean overturning streamfunction over 1850–2014 in the historical simulation and over 2080–2100 in the ScenarioMIP experiments. We use all models available, regardless of whether they conform to an inferred relationship (cf. Weijer et al., 2020) or have unrealistic AMOCs. This allows us to obtain robust relationships between variables by covering a wide range of values.

We estimate the real-world overturning pathways from three global ocean reanalyses that assimilate observations into an ocean model: “GloRanV14” (updated version of “GloSea5” e.g., Baker et al., 2022) over 2000–2021, the “Estimating the Circulation and Climate of the Ocean” (ECCOV4; Cessi, 2019; Forget et al., 2015) over 1992–2015 and a robust diagnostic simulation of Lee et al. (2019) that assimilates long-term averaged hydrographic data. We also use the MOC estimate from the inverse model of Lumpkin and Speer (2007) that uses hydrographic data measured over 1987–1996.

## 2.2. Method to Calculate the Overturning Pathways

We use the method of Baker et al. (2020, 2021) with some modifications to calculate the time-mean overturning pathways of the AMOC, the Atlantic mid-depth overturning cell that is often referred to as the NADW cell (the positive (red) streamfunction in the Atlantic basin in Figure 1a). We call the maximum strength of the AMOC in the North Atlantic, “AMOCmax” (purple box in Figure 1a). We refer to each pathway (Figure 1c and Table S3 in Supporting Information S1) as an upwelling pathway of the AMOC because they quantify the time-mean zonally integrated volume transport that returns deep waters of the AMOC to the surface. These pathways are defined by the processes and regions associated with this upwelling. Since they partition the AMOC upwelling, each pathway is greater than or equal to zero. The water mass density changes along each pathway through water mass transformation (Figure 1c).

To separate the pathways, we use the zonally averaged meridional overturning streamfunction in the Atlantic and Indo-Pacific basins. In the SO, defined as latitudes south of 34.5°S, we use the globally integrated streamfunction (Figure 1). In the SO, the SO winds generate an upper cell and indirectly strengthen a lower eddy-induced cell by tilting the SO isopycnals. We partition the AMOC transport southwards across 34.5°S into that advected into the upper and lower cells of the SO (Figure 1a). The transport into the SO lower cell (“At\_IP<sub>lower</sub>” blue box in Figure 1a) must ultimately upwell in the Indo-Pacific basin, whereas that transported into the upper cell either upwells in the SO and returns to the Atlantic basin (the “Atlantic-SO wind pathway”; “SO\_wind<sub>At</sub>” yellow box) or it is transported by zonal flows into the Indo-Pacific basin (“At\_IP<sub>upper</sub>”; not present in Figure 1, but we account for this pathway, which is important in some models (e.g., Figure S2d in Supporting Information S1)). The total pathway into the Indo-Pacific basin (“At\_IP<sub>total</sub>”) either upwells diffusively in this basin without later upwelling in the SO (the Indo-Pacific diffusive pathway; “IP<sub>diffu</sub>” green box in Figure 1b) or it upwells initially via diffusion and later via the SO upper cell (the Indo-Pacific-SO wind pathway; “SO\_wind<sub>IP</sub>” pink box). The partition of these Indo-Pacific pathways illustrated in Figure 1b is not applicable in all models, for example, if At\_IP<sub>upper</sub> > 0. Thus, we calculate these pathways as residuals (see Equation 1, Equation S5 in Supporting Information S1). We note that a decrease in these Indo-Pacific pathways represent a decrease in the pathway of the AMOC into the Indo-Pacific basin. This can occur without a decrease in Indo-Pacific basin diffusive upwelling, for example, through a decrease in the “cell overlap” between the AMOC and the SO lower cell (Figure 1a). The total SO wind pathway (“SO\_wind<sub>total</sub>” orange box) is the sum of the Atlantic- and Indo-Pacific- SO wind pathways, and it is therefore approximately equal to the total upwelling by the SO upper cell (Figure 1). The Atlantic diffusive pathway (“At<sub>diffu</sub>” gray box) upwells NADW in the Atlantic basin before returning northwards, that is, the streamlines of the AMOC are closed within the Atlantic basin (Figure 1a). The sum of the three main pathways analyzed; the Atlantic diffusive pathway (“At<sub>diffu</sub>”), the Indo-Pacific diffusive pathway (“IP<sub>diffu</sub>”) and the total SO wind pathway (“SO\_wind<sub>total</sub>”), are equal to “AMOC<sub>max</sub>” (Equation 1) because the global overturning streamfunction conserves volume (Figure S2 in Supporting Information S1). These pathways define the processes by which North Atlantic origin waters are returned to the surface; these waters either upwell in the Atlantic or Indo-Pacific basins via diffusion (without later upwelling in the SO; “At<sub>diffu</sub>” and “IP<sub>diffu</sub>”) or they upwell in the SO via the SO winds (“SO\_wind<sub>total</sub>”). We modify the method of Baker et al. (2020, 2021) by separating the total Indo-Pacific pathway (“At\_IP<sub>total</sub>”) into the Indo-Pacific diffusive pathway (“IP<sub>diffu</sub>”) and the Indo-Pacific-SO wind pathway (“SO\_wind<sub>IP</sub>”), and combining the latter pathway with the Atlantic-SO wind pathway (“SO\_wind<sub>At</sub>”) to obtain the total SO wind pathway (“SO\_wind<sub>total</sub>”; Figure 1c). Further modifications to the method of Baker et al. (2020, 2021) and the equations used to calculate the pathways (Equations S1–S10) are described in Supporting Information S1.

We extend the application of the method of Baker et al. (2020, 2021) from equilibrium ocean states to transient ocean states. Although water parcels, or their time-mean net flow, will no longer be advected the entire way along the pathways defined by our method before the MOC and its pathways change, we can still estimate the time-mean MOC pathways over a given time period (e.g., over 2080–2100). We find that changes in the MOC, such as AMOC shoaling in response to GHG forcing, can reduce the pathway of the AMOC into the Indo-Pacific basin, and thus reduce the available pathways for returning waters that sink in the North Atlantic to the surface via upwelling. Our results suggest that the AMOC must transiently weaken by a magnitude related to these changes (likely communicated through wave processes) to satisfy conservation of volume in an incompressible ocean, unless other pathways of the AMOC increase. Hence, transient changes in the MOC remote from, but connected to the North Atlantic by these pathways, can modulate the magnitude of AMOC weakening. The weakening is likely instigated by changes in North Atlantic convection.

Since ocean currents tend to follow isopycnals, the overturning pathways are more accurately represented in density space than in depth space (Hallberg & Gnanadesikan, 2006). We compare the overturning pathways calculated in depth and density space in seven models (Figure S1 in Supporting Information S1). Although there are quantitative differences in density space, we expect our qualitative findings to remain valid (see Supporting Information S1).

### 3. Historical MOC and Overturning Pathways

#### 3.1. MOC

We first examine the historical (1850–2014) overturning streamfunction and the associated overturning pathways. In all models, the Atlantic has a clockwise, mid-depth cell (i.e., the AMOC), whereas the Indo-Pacific has an expansive anti-clockwise cell. The historical AMOC strength (“AMOC<sub>max</sub>”) ranges from ~10 to ~37 Sv, and there is large inter-model spread in the overturning pathways (Figures 2a–2c, Figure S2 in Supporting Information S1). The AMOC has notable multi-decadal variations during the historical period, but all models appear to be sufficiently spun-up (Figure S4 in Supporting Information S1).

#### 3.2. Absolute Overturning Pathways

Since the sum of the Atlantic (“At\_diffu”) and Indo-Pacific (“IP\_diffu”) diffusive pathways and the total SO wind pathway (“SO\_wind<sub>total</sub>”) are equal to “AMOC<sub>max</sub>” (Equation 1), we might expect the historical AMOC strength to correlate with the magnitude of each pathway. While the AMOC strength has a strong, positive correlation with the Atlantic and Indo-Pacific diffusive pathways, it is insignificantly ( $p > 0.05$  in a two-tailed  $t$ -test) anti-correlated with the total SO wind pathway (Figures 2a–2c). This is because there are a cluster of models with weak total SO wind pathways, yet strong AMOCs (left side of Figure 2b) because they have large Indo-Pacific diffusive pathways (right side of Figure 2c). The remaining models show a positive correlation between the AMOC strength and the total SO wind pathway.

#### 3.3. Relative Overturning Pathways

We also find similar relationships, but with lower correlations, between the historical AMOC strength and the overturning pathways relative to this AMOC strength that is, the relative contribution of each pathway to “AMOC<sub>max</sub>” (Figures S5a–S5c in Supporting Information S1). However, the relative total SO wind pathway is significantly anti-correlated with AMOC strength. Thus, models with lower relative total SO wind pathways tend to have stronger AMOCs. The relative total SO wind and relative Indo-Pacific diffusive pathways have similar ranges but opposing relationships with “AMOC<sub>max</sub>” (Figures S5b and S5c in Supporting Information S1). The ensemble-mean relative total SO wind pathway (55%) is greater than the ensemble-mean relative Atlantic (23%) and Indo-Pacific (22%) diffusive pathways (Figures S5a–S5c in Supporting Information S1).

### 4. Transient Response of AMOC and Overturning Pathways to Warming

#### 4.1. AMOC Weakening

The CMIP6 ensemble predicts AMOC weakening over the 21st century under all warming scenarios, but with large inter-model variation. The AMOC weakens by 9%–42% (mean value of 24%) in ssp126 (Figure 2d) and

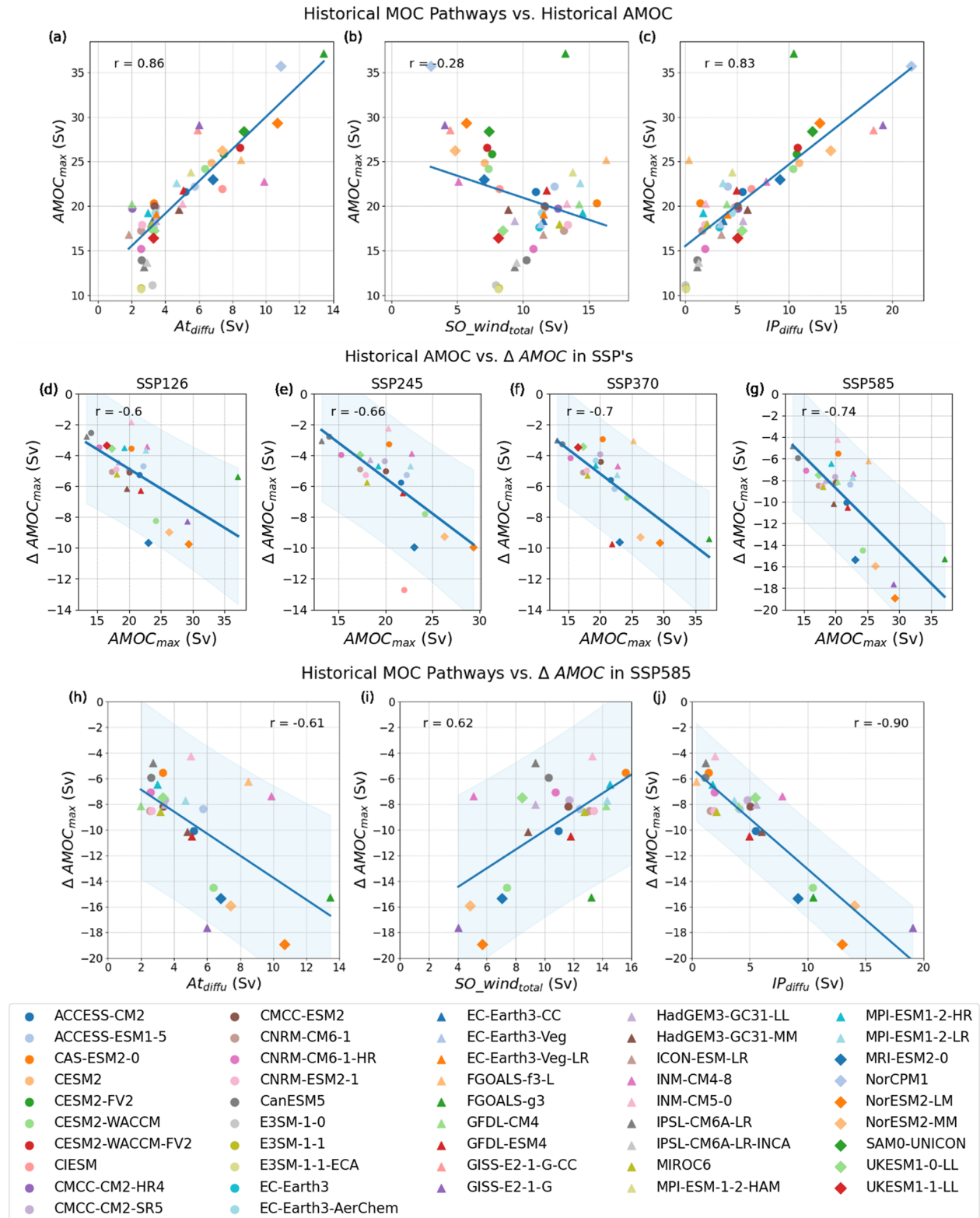


**Figure 2.** (a–c) Overturning pathways calculated in depth space and averaged over the historical simulation (1850–2014), plotted against “AMOC<sub>max</sub>” (d–g) The historical average Atlantic Meridional Overturning Circulation strength, “AMOC<sub>max</sub>” plotted against the change in “AMOC<sub>max</sub>” by 2080–2100 in (d) ssp126 (e) ssp245 (f) ssp370, and (g) ssp585. (h–j) Historical overturning pathways plotted against the change in “AMOC<sub>max</sub>” by 2080–2100 in ssp585. The Atlantic diffusive pathway, “At<sub>diffu</sub>,” the total Southern Ocean wind pathway, “SO<sub>wind</sub><sub>total</sub>” and the Indo-Pacific diffusive pathway, “IP<sub>diffu</sub>” are plotted. The line of best fit and the Pearson correlation coefficient are shown. Blue shading in (d–j) represents the 95% prediction interval.

by 21%–67% (mean value of 44%) in ssp585 by 2080–2100 (Figure 2g), relative to the historical (1850–2014) mean AMOC for each model. Models with a stronger historical AMOC tend to have greater AMOC weakening (Figures 2d–2g), consistent with previous inter-model comparison studies (e.g., Weaver et al., 2012; Weijer et al., 2020; Winton et al., 2014). This relationship strengthens at higher rates of warming, that is, from ssp126 to ssp585. In addition to the AMOC weakening, the Indo-Pacific MOC also weakens (Figure S3 in Supporting Information S1) to conserve volume in each basin, and it therefore compensates for changes in the AMOC (in agreement with Sun et al. (2020)). Changes in the Indo-Pacific MOC could result from heaving that can alter the Indo-Pacific basin stratification (Sun et al., 2020), whereas the vertical diffusivity is unlikely to change greatly.

#### 4.2. Changes in the Overturning Pathways

We analyze how the magnitude of the historical overturning pathways relate to AMOC weakening in ssp585 (Figures 2h–2j). Both the Atlantic and Indo-Pacific diffusive pathways are positively correlated with AMOC weakening (i.e., these pathways tend to be larger in models with greater weakening; note that this is equivalent to a negative correlation with AMOC change). In contrast, the total SO wind pathway is anti-correlated with AMOC weakening. The Indo-Pacific diffusive pathway explains 81% of the variance in AMOC weakening (i.e.,  $r = 0.90$  in ssp585; Figure 2j), notably higher than the 55% of the variance explained by the historical AMOC strength (i.e.,  $r = 0.74$  in ssp585; Figure 2g). The AMOC weakening is less dependent on the Atlantic diffusive and total SO wind pathways ( $r = 0.61$  and  $r = -0.62$  respectively), which reduce its dependence on the historical AMOC strength. Thus, the primary reason for the strong dependence of AMOC weakening on the historical AMOC strength is its strong dependence on the Indo-Pacific diffusive pathway. The aforementioned correlation coefficients are lower for ssp126 than ssp585, but the AMOC weakening still has a higher correlation with the Indo-Pacific diffusive pathway ( $r = 0.78$ , not shown) than with the historical AMOC strength ( $r = 0.6$ ; Figure 2d). We include all models in our analysis to obtain robust relationships, but we also calculate the dependencies when excluding the six-model subset with large Indo-Pacific diffusive pathways (lower right of Figure 2j). This greatly reduces the range of this pathway across the ensemble. The correlation between this pathway and AMOC weakening decreases, but remains significant in ssp585 ( $r = 0.58$ ,  $p < 0.05$ ; not shown), validating our findings. In contrast, AMOC weakening is then insignificantly correlated with the historical AMOC strength ( $r = 0.27$ ,  $p > 0.05$  in ssp585; not shown).

We now examine how the overturning pathways change over the 21st century in ssp585 (Figure 3) to understand why the AMOC weakening depends strongly on the Indo-Pacific diffusive pathway (and less on the other pathways). Although the AMOC weakens in all models, the rate and magnitude of weakening vary greatly (Figures 3a and 3e). By 2100, all models predict a decrease in the Indo-Pacific and Atlantic diffusive pathways, but the total SO wind pathway has a mixed response (Figures 3b–3d and 3f–3h). This pathway typically contributes little to the change in AMOC strength (Figures 3c and 3g) so has little impact on the relationship between the Indo-Pacific diffusive pathway and AMOC weakening. This is because the strength of the SO upper cell at 34.5°S remains relatively unchanged, likely due to the zonal-mean SO westerly wind strength (defined as the maximum value south of 34.5°S) increasing in 92% of the models analyzed for ssp585 by 2080–2100, compensating for their poleward shift in 56% of the models (not shown). By 2100, there is a large variation in the decrease of the Indo-Pacific diffusive pathway across models ( $\sim 1$ –13 Sv), whereas the Atlantic diffusive pathway tends to decrease less (Figure 3). Changes in the Atlantic and Indo-Pacific diffusive pathways are highly correlated ( $r = 0.76$ , not shown).

The AMOC weakening correlates strongly with the decrease in the Atlantic and Indo-Pacific diffusive pathways (Figures S6a and S6c in Supporting Information S1). In contrast, changes in the total SO wind pathway are weakly anti-correlated with AMOC weakening (Figure S6b in Supporting Information S1) due to models with a strong Indo-Pacific diffusive pathway weakening most despite little change in their total SO wind pathways. We also find changes in the Indo-Pacific diffusive pathway are almost inversely proportional to its historical magnitude ( $r = -0.97$ ; not shown), whereas changes in the Atlantic and total SO wind pathways depend less on their historical magnitudes ( $r = -0.7$  and  $r = -0.45$  respectively).

#### 4.3. Mechanisms

The almost proportional relationship between the historical Indo-Pacific diffusive pathway and its decrease by 2080–2100 is due, in part, to this pathway weakening to zero in many models during the 21st century (Figure 3d). The historical magnitude of this pathway sets an upper limit on its weakening. Since changes in this pathway

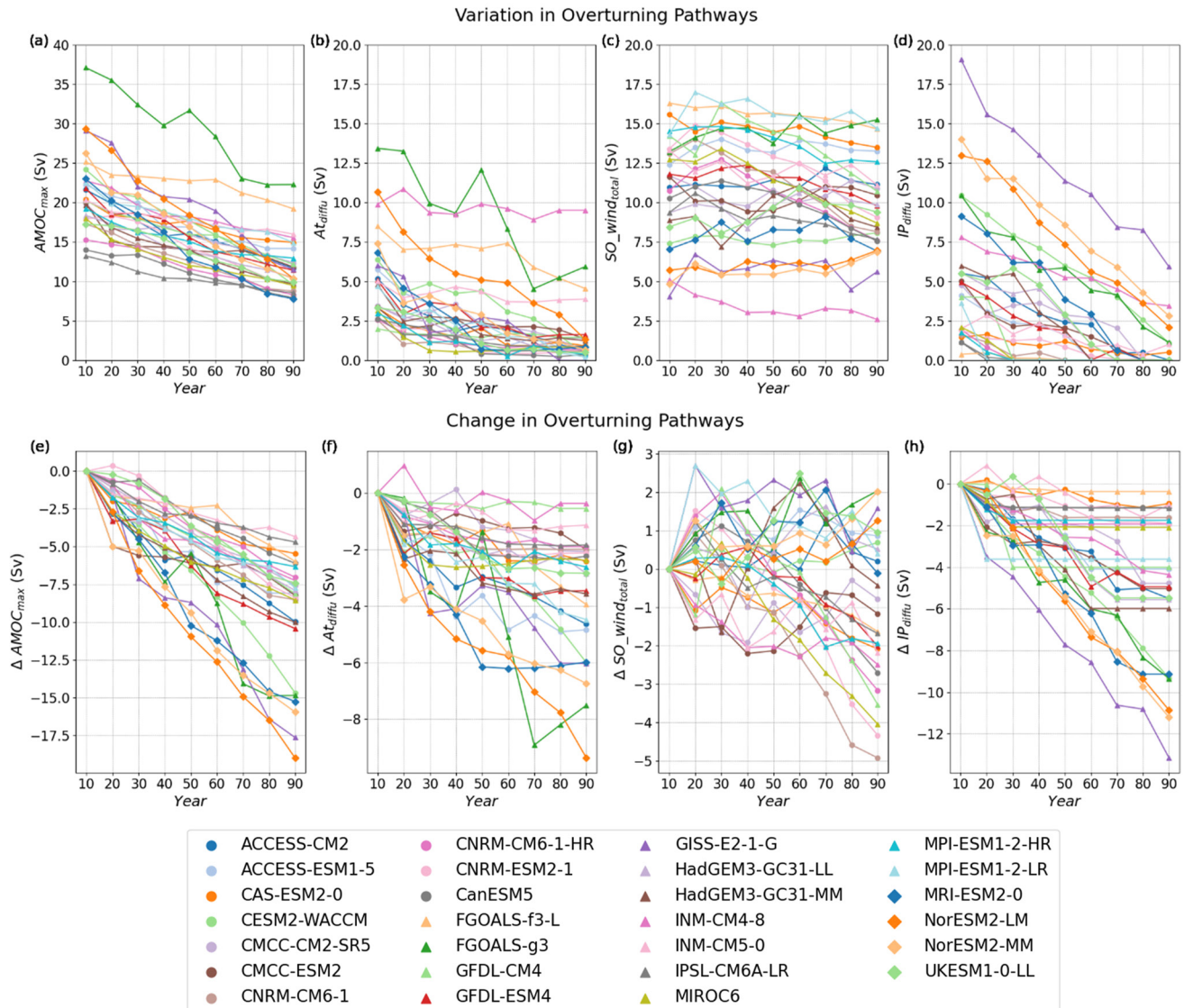


**Figure 3.** Time series of the Atlantic Meridional Overturning Circulation strength and overturning pathways showing (a–d) their absolute magnitudes, and (e–h) the change in their magnitudes from the historical average (1850–2014). The historical average is labeled as 2010 (“10”) with average values in “ssp585” calculated in 10-year intervals from 2015 to 2095 (labeled “20”–“90”).

correlate strongly with changes in the Atlantic diffusive pathway, and the total SO wind pathway is relatively steady, the historical magnitude of the Indo-Pacific diffusive pathway constrains the AMOC’s decline (see Equation 1). Thus, while reduced North Atlantic convection probably causes the AMOC to weaken, the magnitude of decline is modulated by the magnitude of the Indo-Pacific diffusive pathway. This pathway decreases, in part, because the “cell overlap” between the AMOC and the SO lower cell (Figure 1a) decreases in response to GHG forcing, reducing the main pathway of the AMOC into the Indo-Pacific Ocean (Figure S3 in Supporting Information S1; see Baker et al., 2020, 2021; Nadeau & Jansen, 2020). It also decreases because the Indo-Pacific MOC weakens (Figure S3 in Supporting Information S1) to conserve volume as the AMOC weakens due to reduced North Atlantic convection, with changes communicated rapidly via wave processes (Sun et al., 2020).

### 5. Constraining Future AMOC Weakening

Since the AMOC weakening is strongly related to the magnitude of the historical Indo-Pacific diffusive pathway, we use this emergent constraint relationship (i.e., the linear relationship in Figure 2j) to predict future weakening



of the real-world AMOC. Using the AMOC strength and overturning pathways inferred from observation-based MOC estimates (Table S2 in Supporting Information S1), the emergent constraint relationship (Figure 2j) predicts large differences in AMOC decline by 2080–2100 under ssp585 forcing; 29% (range of 8%–50% from the 95% prediction interval in Figure 2j) from ECCOV4, 35% (14%–56%) from an inverse model estimate (Lumpkin & Speer, 2007), 41% (26%–56%) from a robust diagnostic simulation (Lee et al., 2019) and 61% (41%–81%) from GloRanV14 (Table S2 in Supporting Information S1). Under ssp126 forcing, the emergent constraint predicts a weaker AMOC decline for each observation-based estimate, ranging from 17% to 32% (Table S2 in Supporting Information S1).

Although the prediction intervals of the emergent constraint relationship are wide (Figure 2j), they are considerably narrower than an equivalent analysis using the historical AMOC strength to constrain the weakening (Figure 2g). Each of the observation-based estimates of AMOC strength (except the robust diagnostic simulation) and a direct observational estimate at 26.5°N of 16.9 Sv (Moat et al., 2022) imply a weakening under ssp585 forcing of ~41% (6%–76%) by 2080–2100. Despite high confidence in the AMOC strength observed at 26.5°N, AMOC weakening constrained by this estimate is highly uncertain. Thus, even though the Indo-Pacific diffusive pathway is uncertain, AMOC weakening based on this pathway has a comparable uncertainty (8%–81%) to that based on the AMOC strength. Between observation-based estimates, their South Atlantic transports are similar, but their total SO wind pathways and thus Indo-Pacific diffusive pathways differ (Table S2 in Supporting Information S1). Reducing uncertainty in the SO upper cell strength at 34.5°S and thus in these pathways would increase confidence in future AMOC decline.

## 6. Discussion and Conclusions

The response of the AMOC to GHG forcing differs across 27 CMIP6 models. By 2080–2100, under low-end forcing (SSP1-2.6), the AMOC weakens in each model on average by 24% (range of 9%–42% across the multi-model ensemble) relative to its historical mean AMOC, while under high-end forcing (SSP5-8.5), the average weakening increases to 44% (range of 21%–67%). We show that the magnitude of the historical (1850–2014) overturning pathways largely determines how the AMOC responds to future climate forcing. Specifically, the historical pathway of North Atlantic origin waters that upwells diffusively in the Indo-Pacific Ocean but is not later upwelled in the SO is strongly related to the AMOC weakening. Under SSP5-8.5 forcing, this Indo-Pacific diffusive pathway explains 81% of the variance in the AMOC weakening across the ensemble, more than that explained by the historical AMOC strength (55%). We can use this emergent constraint relationship on AMOC weakening to predict future changes in the AMOC, but observation-based estimates of the real-world Indo-Pacific diffusive pathway are uncertain. They imply a wide range of AMOC weakening by 2080–2100 of 17%–32% (best estimates) for SSP1-2.6 and of 29%–61% for SSP5-8.5.

Mechanisms proposed to explain the association between the AMOC weakening and its historical strength (e.g., Cheng et al., 2013; Weaver et al., 2012; Weijer et al., 2020) largely focus on the mean state of the North Atlantic (e.g., Jackson et al., 2020; Levermann et al., 2007). We argue that because AMOC weakening has a stronger dependence on the Indo-Pacific diffusive pathway than the historical AMOC strength, these North Atlantic based mechanisms may not fully explain this relationship. Although changes in North Atlantic convection likely cause the AMOC to shoal and weaken, the magnitude of this weakening is largely controlled by the magnitude of the Indo-Pacific diffusive pathway.

As the AMOC shoals, the “cell overlap” between the AMOC and the SO lower cell decreases, reducing the pathway into the Indo-Pacific Ocean (e.g., Baker et al., 2020, 2021; Nadeau & Jansen, 2020). The weakening of the AMOC is strongly dependent on the historical magnitude of the Indo-Pacific diffusive pathway, in part, because its magnitude acts as an upper limit on its decrease. Changes in the pathway of the AMOC that upwells in the Atlantic are also strongly correlated with changes in the Indo-Pacific diffusive pathway, whereas the pathway that upwells via the SO wind-driven upper cell changes little under GHG forcing.

The structure and strength of the AMOC depends on various factors, such as the buoyancy forcing, the vertical diffusivity, the SO wind stress and mesoscale eddies (Bellomo et al., 2021). The historical overturning pathways are therefore dependent on these model processes and forcings. Thus, models need to represent these processes accurately to simulate a realistic historical MOC and AMOC response. Improved observational estimates of the real-world overturning pathways would reduce uncertainty in our prediction of AMOC weakening. They may

also suggest how to improve climate models' historical MOC and thus AMOC changes, as well as their oceanic transports of heat, salinity and carbon (e.g., Aldama-Campino et al., 2020; Heuzé, 2021; Sun et al., 2022). Future research could explore the cause of the large inter-model spread in the historical overturning pathways and AMOC strength.

## Data Availability Statement

The CMIP6 data used in this study is available from ESGF (<https://esgf-index1.ceda.ac.uk/search/cmip6-ceda/>) with references listed in Supporting Information S1 (Table S1). MOC estimates from ECCOv4, a robust diagnostic simulation and an inverse model were taken from Cessi (2019), Lee et al. (2019), and Lumpkin and Speer (2007) respectively. MOC estimates from GloRanV14 (funded by the E.U. Copernicus Marine Service) are available through Zenodo: <https://doi.org/10.5281/zenodo.7649266> (Baker & Renshaw, 2023).

## Acknowledgments

JAB, LCJ and RAW were supported by the European Union's Horizon 2020 research and innovation programme (Grant 820970, TiPES project). LCJ, MJB, and RAW were supported by the Met Office Hadley Centre Climate Programme funded by BEIS.

## References

- Aldama-Campino, A., Fransner, F., Ödalen, M., Groeskamp, S., Yool, A., Döös, K., & Nycander, J. (2020). Meridional ocean carbon transport. *Global Biogeochemical Cycles*, 34(9), e2019GB006336. <https://doi.org/10.1029/2019GB006336>
- Baker, J., & Renshaw, R. (2023). GloRanV14 ocean reanalysis MOC data [Dataset]. Zenodo. <https://doi.org/10.5281/zenodo.7649266>
- Baker, J. A., Renshaw, R., Jackson, L. C., Dubois, C., Iovino, D., Zuo, H., et al. (2022). Overturning and heat transport variations in the South Atlantic in an ocean reanalysis ensemble. *State Planet Discuss.* [preprint], accepted. <https://doi.org/10.5194/sp-2022-8>
- Baker, J. A., Watson, A. J., & Vallis, G. K. (2020). Meridional overturning circulation in a multibasin model. Part I: Dependence on southern ocean buoyancy forcing. *Journal of Physical Oceanography*, 50(5), 1159–1178. <https://doi.org/10.1175/JPO-D-19-0135.1>
- Baker, J. A., Watson, A. J., & Vallis, G. K. (2021). Meridional overturning circulation in a multibasin model. Part II: Sensitivity to diffusivity and wind in warm and cool climates. *Journal of Physical Oceanography*, 51(6), 1813–1828. <https://doi.org/10.1175/JPO-D-20-0121.1>
- Bellomo, K., Angeloni, M., Corti, S., & von Hardenberg, J. (2021). Future climate change shaped by inter-model differences in Atlantic meridional overturning circulation response. *Nature Communications*, 12(1), 1–10. <https://doi.org/10.1038/s41467-021-24015-w>
- Bonan, D. B., Thompson, A. F., Newsom, E. R., Sun, S., & Rugenstein, M. (2022). Transient and equilibrium responses of the Atlantic overturning circulation to warming in coupled climate models: The role of temperature and salinity. *Journal of Climate*, 35(15), 5173–5193. <https://doi.org/10.1175/jcli-d-21-0912.1>
- Buckley, M. W., & Marshall, J. (2016). Observations, inferences, and mechanisms of the Atlantic meridional overturning circulation: A review. *Reviews of Geophysics*, 54(1), 5–63. <https://doi.org/10.1002/2015RG000493>
- Cessi, P. (2019). The global overturning circulation. *Annual Review of Marine Science*, 11(1), 249–270. <https://doi.org/10.1146/ANNUREV-MARINE-010318-095241>
- Chang, C.-Y., & Jansen, M. F. (2022). The time-dependent response of a two-basin ocean to a sudden surface temperature change. *Journal of Climate*, 35(14), 1–34. <https://doi.org/10.1175/jcli-d-21-0821.1>
- Cheng, W., Chiang, J. C. H., & Zhang, D. (2013). Atlantic meridional overturning circulation (AMOC) in CMIP5 models: RCP and historical simulations. *Journal of Climate*, 26(18), 7187–7197. <https://doi.org/10.1175/JCLI-D-12-00496.1>
- Deng, K., Azorin-Molina, C., Yang, S., Hu, C., Zhang, G., Minola, L., & Chen, D. (2022). Changes of Southern Hemisphere westerlies in the future warming climate. *Atmospheric Research*, 270, 106040. <https://doi.org/10.1016/j.atmosres.2022.106040>
- Dixon, K. W., Delworth, T. L., Spelman, M. J., & Stouffer, R. J. (1999). The influence of transient surface fluxes on North Atlantic overturning in a coupled GCM climate change experiment. *Geophysical Research Letters*, 26(17), 2749–2752. <https://doi.org/10.1029/1999GL900571>
- Eyring, V., Bony, S., Meehl, G. A., Senior, C. A., Stevens, B., Stouffer, R. J., & Taylor, K. E. (2016). Overview of the coupled model intercomparison project phase 6 (CMIP6) experimental design and organization. *Geoscientific Model Development*, 9(5), 1937–1958. <https://doi.org/10.5194/gmd-9-1937-2016>
- Ferrari, R., Jansen, M. F., Adkins, J. F., Burke, A., Stewart, A. L., & Thompson, A. F. (2014). Antarctic sea ice control on ocean circulation in present and glacial climates. *Proceedings of the National Academy of Sciences of the United States of America*, 111(24), 8753–8758. [https://doi.org/10.1073/PNAS.1323922111/SUPPL\\_FILE/PNAS.201323922SI.PDF](https://doi.org/10.1073/PNAS.1323922111/SUPPL_FILE/PNAS.201323922SI.PDF)
- Ferrari, R., Nadeau, L.-P., Marshall, D., Allison, L. C., & Johnson, H. L. (2017). A model of the ocean overturning circulation with two closed basins and a reentrant channel. *Journal of Physical Oceanography*, 47(12), 2887–2906. <https://doi.org/10.1175/JPO-D-16-0223.1>
- Forget, G., Campin, J. M., Heimbach, P., Hill, C. N., Ponte, R. M., & Wunsch, C. (2015). ECCO version 4: An integrated framework for non-linear inverse modeling and global ocean state estimation. *Geoscientific Model Development*, 8(10), 3071–3104. <https://doi.org/10.5194/GMD-8-3071-2015>
- Gregory, J. M., Dixon, K. W., Stouffer, R. J., Weaver, A. J., Driesschaert, E., Eby, M., et al. (2005). A model intercomparison of changes in the Atlantic thermohaline circulation in response to increasing atmospheric CO<sub>2</sub> concentration. <https://doi.org/10.1029/2005GL023209>
- Gregory, J. M., & Tailleux, R. (2011). Kinetic energy analysis of the response of the Atlantic meridional overturning circulation to CO<sub>2</sub>-forced climate change. *Climate Dynamics*, 37(5), 893–914. <https://doi.org/10.1007/S00382-010-0847-6/FIGURES/11>
- Griffies, S. M., Danabasoglu, G., Durack, P. J., Adcroft, A. J., Balaji, V., Böning, C. W., et al. (2016). OMIP contribution to CMIP6: Experimental and diagnostic protocol for the physical component of the Ocean Model Intercomparison Project. *Geoscientific Model Development*, 9(9), 3231–3296. <https://doi.org/10.5194/GMD-9-3231-2016>
- Hallberg, R., & Gnanadesikan, A. (2006). The role of eddies in determining the structure and response of the wind-driven southern hemisphere overturning: Results from the Modeling Eddies in the Southern Ocean (MESO) project. *Journal of Physical Oceanography*, 36(12), 2232–2252. <https://doi.org/10.1175/JPO2980.1>
- Heuzé, C. (2021). Antarctic bottom water and North Atlantic deep water in CMIP6 models. *Ocean Science*, 17(1), 59–90. <https://doi.org/10.5194/os-17-59-2021>
- Hu, A., van Roekel, L., Weijer, W., Garuba, O. A., Cheng, W., & Nadiga, B. T. (2020). Role of AMOC in transient climate response to greenhouse gas forcing in two coupled models. *Journal of Climate*, 33(14), 5845–5859. <https://doi.org/10.1175/JCLI-D-19-1027.1>
- Jackson, L. C., Roberts, M. J., Hewitt, H. T., Iovino, D., Koenigk, T., Meccia, V. L., et al. (2020). Impact of ocean resolution and mean state on the rate of AMOC weakening. *Climate Dynamics*, 55(7–8), 1711–1732. <https://doi.org/10.1007/s00382-020-05345-9>

- Jones, C. S., & Cessi, P. (2016). Interbasin transport of the meridional overturning circulation. *Journal of Physical Oceanography*, 46(4), 1157–1169. <https://doi.org/10.1175/JPO-D-15-0197.1>
- Lee, S. K., Lumpkin, R., Baringer, M. O., Meinen, C. S., Goes, M., Dong, S., et al. (2019). Global meridional overturning circulation inferred from a data-constrained ocean & sea-ice model. *Geophysical Research Letters*, 46(3), 1521–1530. <https://doi.org/10.1029/2018GL080940>
- Levermann, A., Mignot, J., Nawrath, S., & Rahmstorf, S. (2007). The role of northern sea ice cover for the weakening of the thermohaline circulation under global warming. <https://doi.org/10.1175/JCLI4232.1>
- Liu, W., Fedorov, A. V., Xie, S. P., & Hu, S. (2020). Climate impacts of a weakened Atlantic meridional overturning circulation in a warming climate. *Science Advances*, 6(26). [https://doi.org/10.1126/SCIADV.AAZ4876/SUPPL\\_FILE/AAZ4876\\_SM.PDF](https://doi.org/10.1126/SCIADV.AAZ4876/SUPPL_FILE/AAZ4876_SM.PDF)
- Lumpkin, R., & Speer, K. (2007). Global ocean meridional overturning. *Journal of Physical Oceanography*, 37(10), 2550–2562. <https://doi.org/10.1175/JPO3130.1>
- Moat, B. I., Frajka-Williams, E., Smeed, D. A., Rayner, D., Johns, W. E., Baringer, M. O., et al. (2022). Atlantic meridional overturning circulation observed by the RAPID-MOCHA-WBTS (RAPID-meridional Overturning Circulation and Heatflux Array-Western Boundary Time Series) array at 26N from 2004 to 2020 (v2020.2). [Dataset]. British Oceanographic Data Centre, Natural Environment Research Council. <https://doi.org/10.5285/e91b10af-6f0a-7fa7-e053-6c86abc05a09>
- Munk, W., & Wunsch, C. (1998). Abyssal recipes II: Energetics of tidal and wind mixing. *Deep Sea Research Part I: Oceanographic Research Papers*, 45(12), 1977–2010. [https://doi.org/10.1016/S0967-0637\(98\)00070-3](https://doi.org/10.1016/S0967-0637(98)00070-3)
- Nadeau, L. P., & Jansen, M. F. (2020). Overturning circulation pathways in a two-basin ocean model. *Journal of Physical Oceanography*, 50(8), 2105–2122. <https://doi.org/10.1175/JPO-D-20-0034.1>
- Newsom, E. R., & Thompson, A. F. (2018). Reassessing the role of the Indo-Pacific in the ocean's global overturning circulation. *Geophysical Research Letters*, 45(22), 12422–12431. <https://doi.org/10.1029/2018GL080350>
- O'Neill, B. C., Tebaldi, C., van Vuuren, D. P., Eyring, V., Friedlingstein, P., Hurtt, G., et al. (2016). The scenario model intercomparison project (ScenarioMIP) for CMIP6. *Geoscientific Model Development*, 9, 3461–3482. <https://doi.org/10.5194/gmd-9-3461-2016>
- Rahmstorf, S., Box, J. E., Feulner, G., Mann, M. E., Robinson, A., Rutherford, S., & Schaffernicht, E. J. (2015). Exceptional twentieth-century slowdown in Atlantic Ocean overturning circulation. *Nature Climate Change*, 5(5), 475–480. <https://doi.org/10.1038/nclimate2554>
- Riahi, K., van Vuuren, D. P., Kriegler, E., Edmonds, J., O'Neill, B. C., Fujimori, S., et al. (2017). The shared socioeconomic pathways and their energy, land use, and greenhouse gas emissions implications: An overview. *Global Environmental Change*, 42, 153–168. <https://doi.org/10.1016/j.gloenvcha.2016.05.009>
- Rugenstein, M. A. A., Winton, M., Stouffer, R. J., Griffies, S. M., & Hallberg, R. (2013). Northern high-latitude heat budget decomposition and transient warming. *Journal of Climate*, 26(2), 609–621. <https://doi.org/10.1175/JCLI-D-11-00695.1>
- Stouffer, R. J., Yin, J., Gregory, J. M., Dixon, K. W., Spelman, M. J., Hurlin, W., et al. (2006). Investigating the causes of the response of the thermohaline circulation to past and future climate changes. *Journal of Climate*, 19(8), 1365–1387. <https://doi.org/10.1175/JCLI3689.1>
- Sun, S., Thompson, A. F., & Eisenman, I. (2020). Transient overturning compensation between Atlantic and Indo-Pacific basins. *Journal of Physical Oceanography*, 50(8), 2151–2172. <https://doi.org/10.1175/JPO-D-20-0060.1>
- Sun, S., Thompson, A. F., Xie, S. P., & Long, S. M. (2022). Indo-Pacific warming induced by a weakening of the Atlantic meridional overturning circulation. *Journal of Climate*, 35(2), 815–832. <https://doi.org/10.1175/JCLI-D-21-0346.1>
- Talley, L. D. (2013). Closure of the global overturning circulation through the Indian, Pacific, and southern oceans. *Oceanography*, 26(1), 80–97. <https://doi.org/10.5670/OCEANOLOG.2013.07>
- Thompson, A. F., Stewart, A. L., & Bischoff, T. (2016). A multibasin residual-mean model for the global overturning circulation. *Journal of Physical Oceanography*, 46(9), 2583–2604. <https://doi.org/10.1175/JPO-D-15-0204.1>
- Toggweiler, J. R., & Samuels, B. (1998). On the ocean's large-scale circulation near the limit of no vertical mixing. *Journal of Physical Oceanography*, 28(9), 1832–1852. [https://doi.org/10.1175/1520-0485\(1998\)028](https://doi.org/10.1175/1520-0485(1998)028)
- Weaver, A. J., Sedláček, J., Eby, M., Alexander, K., Crespin, E., Fichefet, T., et al. (2012). Stability of the Atlantic meridional overturning circulation: A model intercomparison. *Geophysical Research Letters*, 39(20), 20709. <https://doi.org/10.1029/2012GL053763>
- Weijer, W., Cheng, W., Drijfhout, S. S., Fedorov, A. V., Hu, A., Jackson, L. C., et al. (2019). Stability of the Atlantic meridional overturning circulation: A review and synthesis. *Journal of Geophysical Research: Oceans*, 124(8), 5336–5375. <https://doi.org/10.1029/2019JC015083>
- Weijer, W., Cheng, W., Garuba, O. A., Hu, A., & Nadiga, B. T. (2020). CMIP6 models predict significant 21st century decline of the Atlantic meridional overturning circulation. *Geophysical Research Letters*, 47(12), e2019GL086075. <https://doi.org/10.1029/2019GL086075>
- Winton, M., Anderson, W. G., Delworth, T. L., Griffies, S. M., Hurlin, W. J., & Rosati, A. (2014). Has coarse ocean resolution biased simulations of transient climate sensitivity? *Geophysical Research Letters*, 41(23), 8522–8529. <https://doi.org/10.1002/2014GL061523>

## References From the Supporting Information

- Andrews, M. B., Ridley, J. K., Wood, R. A., Andrews, T., Blockley, E. W., Booth, B., et al. (2020). Historical simulations with HadGEM3-GC3.1 for CMIP6. *Journal of Advances in Modeling Earth Systems*, 12(6), e2019MS001995. <https://doi.org/10.1029/2019MS001995>
- Bethke, I., Wang, Y., Counillon, F., Keenlyside, N., Kimmritz, M., Fransner, F., et al. (2021). NorCPM1 and its contribution to CMIP6 DCCP. *Geoscientific Model Development*, 14(11), 7073–7116. <https://doi.org/10.5194/GMD-14-7073-2021>
- Bi, D., Dix, M., Marsland, S., O'farrell, S., Sullivan, A., Bodman, R., et al. (2020). Configuration and spin-up of ACCESS-CM2, the new generation Australian community climate and Earth system simulator coupled model. *Journal of Southern Hemisphere Earth Systems Science*, 70(1), 225–251. <https://doi.org/10.1071/ES19040>
- Boucher, O., Servonnat, J., Albright, A. L., Aumont, O., Balkanski, Y., Bastrikov, V., et al. (2020). Presentation and evaluation of the IPSL-CM6A-LR climate model. *Journal of Advances in Modeling Earth Systems*, 12(7). <https://doi.org/10.1029/2019MS002010>
- Cherchi, A., Fogli, P. G., Lovato, T., Peano, D., Iovino, D., Gualdi, S., et al. (2019). Global mean climate and main patterns of variability in the CMCC-CM2 coupled model. *Journal of Advances in Modeling Earth Systems*, 11(1), 185–209. <https://doi.org/10.1029/2018MS001369>
- Danabasoglu, G., Lamarque, J. F., Bacmeister, J., Bailey, D. A., DuVivier, A. K., Edwards, J., et al. (2020). The community Earth system model version 2 (CESM2). *Journal of Advances in Modeling Earth Systems*, 12(2), e2019MS001916. <https://doi.org/10.1029/2019MS001916>
- Dunne, J. P., Horowitz, L. W., Adcroft, A. J., Ginoux, P., Held, I. M., John, J. G., et al. (2020). The GFDL Earth system model version 4.1 (GFDL-ESM4.1): Overall coupled model description and simulation characteristics. *Journal of Advances in Modeling Earth Systems*, 12(11), e2019MS002015. <https://doi.org/10.1029/2019MS002015>
- Golaz, J. C., Caldwell, P. M., van Roekel, L. P., Petersen, M. R., Tang, Q., Wolfe, J. D., et al. (2019). The DOE E3SM coupled model version 1: Overview and evaluation at standard resolution. *Journal of Advances in Modeling Earth Systems*, 11(7), 2089–2129. <https://doi.org/10.1029/2018MS001603>

- Gutjahr, O., Putrasahan, D., Lohmann, K., Jungclaus, J. H., von Storch, J. S., Brüggemann, N., et al. (2019). Max Planck institute Earth system model (MPI-ESM1.2) for the high-resolution model intercomparison project (HighResMIP). *Geoscientific Model Development*, *12*(7), 3241–3281. <https://doi.org/10.5194/GMD-12-3241-2019>
- He, B., Yu, Y., Bao, Q., Lin, P., Liu, H., Li, J., et al. (2020). CAS FGOALS-f3-L model dataset descriptions for CMIP6 DECK experiments (pp. 582–588). New Pub: KeAi. <https://doi.org/10.1080/16742834.2020.1778419>
- Held, I. M., Guo, H., Adcroft, A., Dunne, J. P., Horowitz, L. W., Krasting, J., et al. (2019). Structure and performance of GFDL's CM4.0 climate model. *Journal of Advances in Modeling Earth Systems*, *11*(11), 3691–3727. <https://doi.org/10.1029/2019MS001829>
- Jungclaus, J. H., Lorenz, S. J., Schmidt, H., Brovkin, V., Brüggemann, N., Chegini, F., et al. (2022). The ICON Earth system model version 1.0. *Journal of Advances in Modeling Earth Systems*, *14*(4), e2021MS002813. <https://doi.org/10.1029/2021MS002813>
- Kelley, M., Schmidt, G. A., Nazarenko, L. S., Bauer, S. E., Ruedy, R., Russell, G. L., et al. (2020). GISS-E2.1: Configurations and climatology. *Journal of Advances in Modeling Earth Systems*, *12*(8), e2019MS002025. <https://doi.org/10.1029/2019MS002025>
- Kuhlbrodt, T., Jones, C. G., Sellar, A., Storkey, D., Blockley, E., Stringer, M., et al. (2018). The low-resolution version of HadGEM3 GC3.1: Development and evaluation for global climate. *Journal of Advances in Modeling Earth Systems*, *10*(11), 2865–2888. <https://doi.org/10.1029/2018MS001370>
- Li, L., Yu, Y., Tang, Y., Lin, P., Xie, J., Song, M., et al. (2020). The flexible global ocean-atmosphere-land system model grid-point version 3 (FGOALS-g3): Description and evaluation. *Journal of Advances in Modeling Earth Systems*, *12*(9), e2019MS002012. <https://doi.org/10.1029/2019MS002012>
- Lin, Y., Huang, X., Liang, Y., Qin, Y., Xu, S., Huang, W., et al. (2020). Community integrated Earth system model (CIESM): Description and evaluation. *Journal of Advances in Modeling Earth Systems*, *12*(8), e2019MS002036. <https://doi.org/10.1029/2019MS002036>
- Lovato, T., Peano, D., Butenschön, M., Materia, S., Iovino, D., Scoccimarro, E., et al. (2022). CMIP6 simulations with the CMCC Earth system model (CMCC-ESM2). *Journal of Advances in Modeling Earth Systems*, *14*(3), e2021MS002814. <https://doi.org/10.1029/2021MS002814>
- Lurton, T., Balkanski, Y., Bastrikov, V., Bekki, S., Bopp, L., Braconnot, P., et al. (2020). Implementation of the CMIP6 forcing data in the IPSL-CM6A-LR model. *Journal of Advances in Modeling Earth Systems*, *12*(4), e2019MS001940. <https://doi.org/10.1029/2019MS001940>
- Mauritsen, T., Bader, J., Becker, T., Behrens, J., Bittner, M., Brokopf, R., et al. (2019). Developments in the MPI-M Earth system model version 1.2 (MPI-ESM1.2) and its response to increasing CO<sub>2</sub>. *Journal of Advances in Modeling Earth Systems*, *11*(4), 998–1038. <https://doi.org/10.1029/2018MS001400>
- Müller, W. A., Jungclaus, J. H., Mauritsen, T., Baehr, J., Bittner, M., Budich, R., et al. (2018). A higher-resolution version of the Max Planck institute Earth system model (MPI-ESM1.2-HR). *Journal of Advances in Modeling Earth Systems*, *10*(7), 1383–1413. <https://doi.org/10.1029/2017MS001217>
- Park, S., Shin, J., Kim, S., Oh, E., & Kim, Y. (2019). Global climate simulated by the Seoul National University atmosphere model version 0 with a unified convection scheme (SAM0-UNICON). *Journal of Climate*, *32*(10), 2917–2949. <https://doi.org/10.1175/JCLI-D-18-0796.1>
- Séférian, R., Nabat, P., Michou, M., Saint-Martin, D., Voldoire, A., Colin, J., et al. (2019). Evaluation of CNRM Earth system model, CNRM-ESM2-1: Role of Earth system processes in present-day and future climate. *Journal of Advances in Modeling Earth Systems*, *11*(12), 4182–4227. <https://doi.org/10.1029/2019MS001791>
- Sellar, A. A., Jones, C. G., Mulcahy, J. P., Tang, Y., Yool, A., Wiltshire, A., et al. (2019). UKESM1: Description and evaluation of the U.K. Earth system model. *Journal of Advances in Modeling Earth Systems*, *11*(12), 4513–4558. <https://doi.org/10.1029/2019MS001739>
- Swart, N. C., Cole, J. N. S., Kharin, V. V., Lazare, M., Scinocca, J. F., Gillett, N. P., et al. (2019). The Canadian Earth system model version 5 (CanESM5.0.3). *Geoscientific Model Development*, *12*(11), 4823–4873. <https://doi.org/10.5194/GMD-12-4823-2019>
- Tatebe, H., Ogura, T., Nitta, T., Komuro, Y., Oguchi, K., Takemura, T., et al. (2019). Description and basic evaluation of simulated mean state, internal variability, and climate sensitivity in MIROC6. *Geoscientific Model Development*, *12*(7), 2727–2765. <https://doi.org/10.5194/GMD-12-2727-2019>
- Tjiputra, J. F., Schwinger, J., Bentsen, M., Morée, A. L., Gao, S., Bethke, I., et al. (2020). Ocean biogeochemistry in the Norwegian Earth system model version 2 (NorESM2). *Geoscientific Model Development*, *13*(5), 2393–2431. <https://doi.org/10.5194/GMD-13-2393-2020>
- Voldoire, A., Saint-Martin, D., Sénési, S., Decharme, B., Alias, A., Chevallier, M., et al. (2019). Evaluation of CMIP6 DECK experiments with CNRM-CM6-1. *Journal of Advances in Modeling Earth Systems*, *11*(7), 2177–2213. <https://doi.org/10.1029/2019MS001683>
- Volodin, E., & Gritsun, A. (2018). Simulation of observed climate changes in 1850–2014 with climate model INM-CM5. *Earth System Dynamics*, *9*(4), 1235–1242. <https://doi.org/10.5194/esd-9-1235-2018>
- Volodin, E. M., Mortikov, E. V., Kostykin, S. V., Galin, V. Y., Lykosov, V. N., Gritsun, A. S., et al. (2018). Simulation of the modern climate using the INM-CM48 climate model. *Russian Journal of Numerical Analysis and Mathematical Modelling*, *33*(6), 367–374. <https://doi.org/10.1515/RNAM-2018-0032/MACHINEREREADABLECITATION/RIS>
- Williams, K. D., Copsey, D., Blockley, E. W., Bodas-Salcedo, A., Calvert, D., Comer, R., et al. (2018). The Met Office global coupled model 3.0 and 3.1 (GC3.0 and GC3.1) configurations. *Journal of Advances in Modeling Earth Systems*, *10*(2), 357–380. <https://doi.org/10.1002/2017MS001115>
- Wyser, K., van Noije, T., Yang, S., von Hardenberg, J., O'Donnell, D., & Döschner, R. (2020). On the increased climate sensitivity in the EC-Earth model from CMIP5 to CMIP6. *Geoscientific Model Development*, *13*(8), 3465–3474. <https://doi.org/10.5194/GMD-13-3465-2020>
- Yukimoto, S., Kawai, H., Koshiro, T., Oshima, N., Yoshida, K., Urakawa, S., et al. (2019). The meteorological research institute Earth system model version 2.0, MRI-ESM2.0: Description and basic evaluation of the physical component. *Journal of the Meteorological Society of Japan. Series II*, *97*(5), 931–965. <https://doi.org/10.2151/JMSJ.2019-051>
- Zhang, H., Zhang, M., Jin, J., Fei, K., Ji, D., Wu, C., et al. (2020). Description and climate simulation performance of CAS-ESM version 2. *Journal of Advances in Modeling Earth Systems*, *12*(12), e2020MS002210. <https://doi.org/10.1029/2020MS002210>
- Ziehn, T., Chamberlain, M. A., Law, R. M., Lenton, A., Bodman, R. W., Dix, M., et al. (2020). The Australian Earth system model: ACCESS-ESM1.5. *Journal of Southern Hemisphere Earth Systems Science*, *70*(1), 193–214. <https://doi.org/10.1071/ES19035>
- Ziehn, T., Lenton, A., Law, R. M., Matear, R. J., & Chamberlain, M. A. (2017). The carbon cycle in the Australian community climate and Earth system simulator (ACCESS-ESM1)—Part 2: Historical simulations. *Geoscientific Model Development*, *10*(7), 2591–2614. <https://doi.org/10.5194/GMD-10-2591-2017>